ICA 2016 BUENOS AIRES
Buenos Aires – 5 to 9 September 2016
Acoustics for the 21st Century...

PROCEEDINGS of the 22nd International Congress on Acoustics

General Musical Acoustics: Paper ICA2016-601

Comments on travelling wave solutions in nonlinear acoustic tubes: Application to musical acoustics

R Harrison[(a)], S Bilbao[(b)]

[(a)]Acoustics and Audio Group, The University of Edinburgh, United Kingdom, r.l.harrison-3@sms.ed.ac.uk
[(b)]Acoustics and Audio Group, The University of Edinburgh, United Kingdom, s.bilbao@ed.ac.uk

Abstract

A common approach to modeling nonlinear behavior in acoustic tubes of variable cross section is to use an uncoupled travelling wave solution whose profile distorts progressively - the distortion occurs due to changes in wave speed, which is a result of the nonlinearity within the system. However, these uncoupled solutions neglect a) any interaction between the waves, even in the cylindrical case, and b) any scattering effects due to changes in cross sectional area. This paper attempts to identify what effect this separation of travelling wave solutions has compared to a coupled-wave solution. This is done with simple numerical time stepping methods for case a) to show the overall deviation of the solution when interactions are neglected. For case b) dispersion analysis is used on the linearized system to highlight the effect of scattering on the dynamics of the system.

Keywords: Nonlinear, Acoustic Tubes, Separable Waves

Comments on travelling wave solutions in nonlinear acoustic tubes: Application to musical acoustics

1 Introduction

It has been known for decades that waves propagating within brass instruments require a nonlinear description. These nonlinearities are responsible for the characteristic 'brassy' sounds produced by these instruments played at high dynamic levels. The theory of nonlinear wave propagation in tubes dates back to at least the 19th century [1]. However, it wasn't until the second half of the 20th century that this theory was applied in musical acoustics. Beauchamp [2] was one of the first to suggest that nonlinearities were present within a brass instrument, modelling the effect through the use of an amplitude dependent high pass filter. However, he did not give an explicit mechanism for the nonlinearity. Later, Hirschberg *et al.* [3] directly measured shock waves in trombones produced by the nonlinearity in wave propagation. Since then, attempts to model this process have focussed on the use of separable nonlinear wave equations, with particular interest on how the wave distorts as it travels from the mouthpiece to the end of the instrument. By "separable" wave equations, we mean that the solutions travel in one direction only and there is no interaction between the forwards and backwards solutions.

Menguy and Gilbert [4] used perturbation techniques on the Euler equations to arrive at a one-dimensional propagation model that describes weakly nonlinear wave propagation with viscous and thermal losses in a cylinder. The nonlinearity and losses in the model were treated as small and become part of the higher order terms in the perturbation expansion. This leaves the one-dimensional wave equation as the zeroth order solution, which permits separable waves. The zeroth order solution is then used in the higher order expansions to include the nonlinearity and losses — the effect of adding these terms results in a generalised Burgers equation in a modified coordinate system. The same techniques were used later for a tube of varying cross sectional area [5]. The change in cross section is also treated as a perturbation to the system, which means that the solutions are still separable. This model was later used in work on measuring the spectral enrichment, or brassiness, of brass instruments [6].

Lombard *et al.* [7] proposed a travelling wave solution for a horn using simple waves and the loss model presented by Menguy and Gilbert. The nonlinearity in this model is that of the inviscid Burgers equation which, when compared in the same coordinate system, is different to the nonlinearity in the Menguy and Gilbert model.

Hybrid linear/nonlinear methods were employed in a frequency domain model by Thompson and Strong [8]. They used a simulated linear reflection function to separate forwards and backwards pressure waves in the mouthpiece of the instrument from measurements of a played trombone. The outward going wave is then modified using a Burgers equation in a series of concatenated tubes — thus including effects due to changes in cross sectional area. Vergez and Rodet [9] used a similar approach in the time domain using reflection functions measured from real instruments but also included a physical model of the lip reed.

The nonlinear models mentioned above are sensible descriptions for experiments that use a high frequency input signal, where it can be assumed little energy is reflected either at a change of cross section or at the radiating end, and the aim is to investigate how a signal is transformed

from input to output. These models will start to break down if they are used as a full description of the system as scattering due to a change in cross section is not taken into account. The hybrid methods do include these effects although they require a linear description to begin with in order to separate the waves at the entrance of the mouthpiece. Furthermore, even in the case of the cylinder there is coupling between forwards and backwards waves. Kausel and Geyer [10] used digital waveguides [11] to model nonlinear wave propagation that included coupling between the forwards and backwards waves through the wave speed. The nonlinearity was created by modulating the delay time between elements, which was controlled by the local change in wave speed.

The aim of this paper is to compare separable and non separable models of nonlinear wave propagation. To begin, in Section 2, analysis of the characteristics of the Euler equations is performed to show that waves are coupled through the wave speed and the change in cross sectional area, and comparisons are made to separable wave models. Numerical experiments are performed in Section 3 using a simple finite-difference scheme to highlight the effect of the wave speed coupling in a cylinder. In Section 4, the linearised equations for coupled and separable waves are then analysed for the case of an exponential horn. Finally, conclusions are presented and some speculations are made on how this coupling affects the overall behaviour of the system.

2 Coupled and uncoupled models

In this section, there and thereafter in this paper, we consider the simplified case of lossless, nonlinear wave propagation within acoustic tubes of variable cross sectional area.

2.1 Model 1 - The Euler equations and coupled waves

The dynamics of an acoustic tube with varying cross sectional area, $S(x)$, can be described in one dimension using the Euler equations that include the cross sectional area term [12]

$$S\partial_t \rho_{tot} + \partial_x (S\rho_{tot} v) = 0, \quad \partial_t (S\rho_{tot} v) + \partial_x \left(S\rho_{tot} v^2\right) + S\partial_x P_{tot} = 0 \tag{1}$$

where $\rho_{tot}(x,t)$ is the total air density at time t and coordinate x, $v(x,t)$ is the particle velocity and $P_{tot}(x,t)$ is the total air pressure. ∂_t and ∂_x denote partial differentiation with respect to time and axial coordinate. In this simple study the spatial domain is taken to be $x \in \mathbb{R}$.

Total density and pressure are made up of static, P_0 and ρ_0, and acoustic, $p(x,t)$ and $\rho(x,t)$, terms so that

$$P_{tot} = P_0 + p, \quad \rho_{tot} = \rho_0 + \rho \tag{2}$$

Equations (1) can be rewritten in terms of pressure and velocity using the adiabatic gas law $P_{tot} = \kappa \rho_{tot}^{\gamma}$, where γ is the ratio of specific heats and $\kappa = P_0/\rho_0^{\gamma}$. This gives

$$\partial_t p + v\partial_x p + \gamma (P_0 + p)\partial_x v + \gamma v (P_0 + p)\frac{S'}{S} = 0 \tag{3a}$$

$$\partial_t v + v\partial_x v + \frac{1}{\rho_0}\left(1+\frac{p}{P_0}\right)^{-\frac{1}{\gamma}}\partial_x p = 0 \tag{3b}$$

where $S' = dS/dx$.

Defining the speed of sound as $c = \sqrt{\gamma\kappa P_{tot}^{1-\frac{1}{\gamma}}}$ and combining equations (3a) and (3b) gives

$$\left[\partial_t + (v \pm c)\,\partial_x\right]\left\{v \pm \frac{2}{\gamma-1}c\right\} = \mp cv\frac{S'}{S} \tag{4}$$

Equation (4) is in the form of a Riemann invariant, where the terms within {} are the invariants which are usually considered to be constant on curves which are sometimes referred to as characteristics. This equation shows that the waves are coupled by the change in cross sectional area and by the change in wave speed given by $v \pm c$.

2.2 Model 2 - Travelling waves from perturbation techniques

Menguy [5] arrived at a separated wave equation first by non-dimensionalising the Euler equations which have been averaged over S and neglecting higher order terms in Mach number — the effect of which linearises the coupling of waves due to the change in area (right hand side of (4)). The method of multiple scales is then applied to the nondimensionalised system. The application of this perturbation technique assumes that the nonlinearity and the rate of change of cross sectional area are both small and therefore considered as higher order terms. This means that to zeroth order, the system is just the linear wave equation with separable wave solutions and coefficients that are slowly changed by the nonlinearity and the change of tube cross section. The distortion of the wave solutions is obtained from the generalised Burgers equation in a modified coordinate system

$$\partial_\sigma q^\pm = \pm q^\pm \partial_{\theta^\pm} q^\pm \mp \frac{q^\pm}{2S}\frac{dS}{d\sigma} \tag{5}$$

where $q^\pm(\sigma,\theta^\pm)$ are the forwards and backwards waves, $\sigma = \frac{\gamma+1}{2c_0}x$ is a scaled length coordinate, $\theta^\pm = t \mp \frac{x}{c_0}$ are the characteristic variables of the forwards and backwards waves and $c_0 = \sqrt{\gamma\kappa P_0^{1-\frac{1}{\gamma}}}$ is the linear speed of sound. The particle velocity and acoustic pressure are given by

$$v = c_0\left(q^+ - q^-\right), \quad p = \rho_0 c_0^2\left(q^+ + q^-\right) \tag{6}$$

Note that the model presented here is dimensionalised so that both of the dependent variables are time like whereas in the original publication it is presented in a nondimensionalised form. Using

$$\partial_\sigma = \frac{2}{(\gamma+1)}\left(c_0\partial_x \pm \partial_t\right), \quad \partial_{\theta^\pm} = \partial_t \tag{7}$$

transforms (5) into

$$\left[\left(1-\frac{\gamma+1}{2}q^{\pm}\right)\partial_t \pm c_0\partial_x\right]q^{\pm} = -c_0\frac{q^{\pm}}{2}\frac{S'}{S} \tag{8}$$

The invariants, $q^{\pm}$, are still a combination of acoustic variables, as in (4), but the nonlinearity appears in the time derivative rather than the spatial derivative. The right hand side of (8) also always uses the negative of the gradient of cross section, regardless of which direction the waves are travelling. Combining (8) gives

$$\partial_t p - \rho_0 c_0^2\left(\frac{\gamma+1}{8}\right)\partial_t\left(\left(\frac{p}{\rho_0 c_0^2}\right)^2+\left(\frac{v}{c_0}\right)^2\right)+\rho_0 c_0^2\partial_x v+\frac{c_0 p}{2}\frac{S'}{S}=0 \tag{9a}$$

$$\partial_t v - \frac{\gamma+1}{4\rho_0 c_0^2}\partial_t(pv)+\frac{1}{\rho_0}\partial_x p+\frac{c_0 v}{2}\frac{S'}{S}=0 \tag{9b}$$

2.3 Model 3 -Travelling velocity waves

The model used by Lombard *et al.* [7] is

$$\left[\partial_t+\left(\frac{\gamma+1}{2}v^{\pm}\pm c_0\right)\partial_x\right]v^{\pm} = \mp c_0 v^{\pm}\frac{S'}{S} \tag{10}$$

where $v^{\pm}(x,t)$ are forwards and backwards velocity waves. This can be seen as a simplification of (4) where the speed of sound is related to the particle velocity by

$$c = c_0 \pm \frac{\gamma-1}{2}v \tag{11}$$

where the coupling due to the change in cross sectional area is linearised. Equation (10) is an uncoupled wave system where the nonlinearity is that of the standard Burgers equation. Local pressure and velocity is given by

$$p = \rho_0 c_0(v^+ - v^-), \quad v = v^+ + v^- \tag{12}$$

Combining (10) gives

$$\partial_t p+\rho_0 c_0^2\partial_x v+\frac{\gamma+1}{4}\partial_x(pv)+\rho_0 c_0^2 v\frac{S'}{S}=0 \tag{13a}$$

$$\partial_t v+\frac{1}{\rho_0}\partial_x p+\frac{\gamma+1}{8}\partial_x\left(v^2+\frac{p^2}{\rho_0^2 c_0^2}\right)+\frac{p}{\rho_0}\frac{S'}{S}=0 \tag{13b}$$

3 Case a: The interaction of travelling waves

This section presents a simple numerical experiment to investigate the effect of interacting waves in a cylindrical tube.

3.1 A simple finite-difference scheme

Consider a finite cylindrical tube of length L so that $x \in [0, L]$ and $S' = 0$. The pressure and velocity fields are sampled on interleaved grids so that $p_l^n = p(l\Delta x, n\Delta t)$ and $v_{l+\frac{1}{2}}^{n+\frac{1}{2}} = v\left(\left(l+\frac{1}{2}\right)\Delta x, \left(n+\frac{1}{2}\right)\Delta t\right)$, where Δx and Δt are the length and time steps, and l and n are integers that index the length position and time step so that $x = l\Delta x$ and $t = n\Delta t$. The spatial domain has $N = \text{floor}(L/h)$ grid points. Discrete operators are defined using spatial and temporal shift operators and approximate either continuous derivatives or averages used to centre the scheme. See [13] for further discussion on interleaved grids and the finite difference operators used for modelling brass instruments. Spatial shift operators act so that $e_{x\pm} p_l^n = p_{l\pm1}^n$ and temporal shift operators $e_{t\pm} p_l^n = p_l^{n\pm1}$. The difference and averaging operators are

$$\delta_{t\cdot} = \frac{e_{t+} - e_{t-}}{2\Delta t}, \quad \delta_{x\cdot} = \frac{e_{x+} - e_{x-}}{2\Delta x}, \quad \delta_{x+} = \frac{e_{x+} - 1}{\Delta x}, \quad \delta_{x-} = \frac{1 - e_{x-}}{\Delta x} \tag{14}$$

$$\mu_{t+} = \frac{e_{t+} + 1}{2}, \quad \mu_{t-} = \frac{1 + e_{t-}}{2}, \quad \mu_{x+} = \frac{e_{x+} + 1}{2}, \quad \mu_{x-} = \frac{1 + e_{x-}}{2} \tag{15}$$

A simple finite difference scheme for Model 1 (equations (3)) is

$$\delta_{t\cdot} p_l^n + \delta_{x\cdot} p_l^n \mu_{x-}\mu_{t-} v_{l+\frac{1}{2}}^{n+\frac{1}{2}} + \gamma\left(P_0 + p_l^n\right)\mu_{t-}\delta_{x-} v_{l+\frac{1}{2}}^{n+\frac{1}{2}} = 0 \tag{16a}$$

$$\delta_{t\cdot} v_{l+\frac{1}{2}}^{n+\frac{1}{2}} + v_{l+\frac{1}{2}}^{n+\frac{1}{2}} \delta_{x\cdot} v_{l+\frac{1}{2}}^{n+\frac{1}{2}} + \frac{1}{\rho_0}\left(1 + \frac{\mu_{t+}\mu_{x+} p_l^n}{P_0}\right)^{-1/\gamma} \mu_{t+}\delta_{x+} p_l^n = 0 \tag{16b}$$

3.2 Numerical results

Numerical experiments are performed to investigate the effect of the coupling of forwards and backwards waves on the distortion of the wave profile before a shock wave is generated. Two test cases are considered that both use scheme (16). The first, Test 1, involves exciting p_0^n and p_N^n with the same excitation signal so that waves interact in the centre of the tube. In the second case, Test 2, only p_0^n is excited and $p_N^n = 0$ so that only one wave is present in the tube — this is equivalent to using a separable wave solution but without making any further assumptions about the system. The pressure profiles of these two cases are presented in Figure 1 after the initial pulse has been established. Experiments are also performed for Test 2 using the linearised form of (16).

Simulations are run at a sample rate of 100 kHz and at a temperature of $28.65°$C. The length spacing is set using $\Delta x = c_0 \Delta t / \lambda$, where the Courant condition is $\lambda = 0.9$. A Hann pulse of length 2 ms and amplitude of 6% of atmospheric pressure was used as a pressure excitation signal. The length of the tube was 4 m. For $l = 0$ and $l = N$, the linearised version of Equation (16b) was used to avoid accessing samples outside of the domain. Simulations were run so that the waves could travel to the end of the tube and the pressure was recorded at $x = 2.8$ m (70% of the tube length) which allowed for a full pulse to be captured. These pressure signals are presented at top of Figure 2. The Fourier transforms of these pressure signals are presented

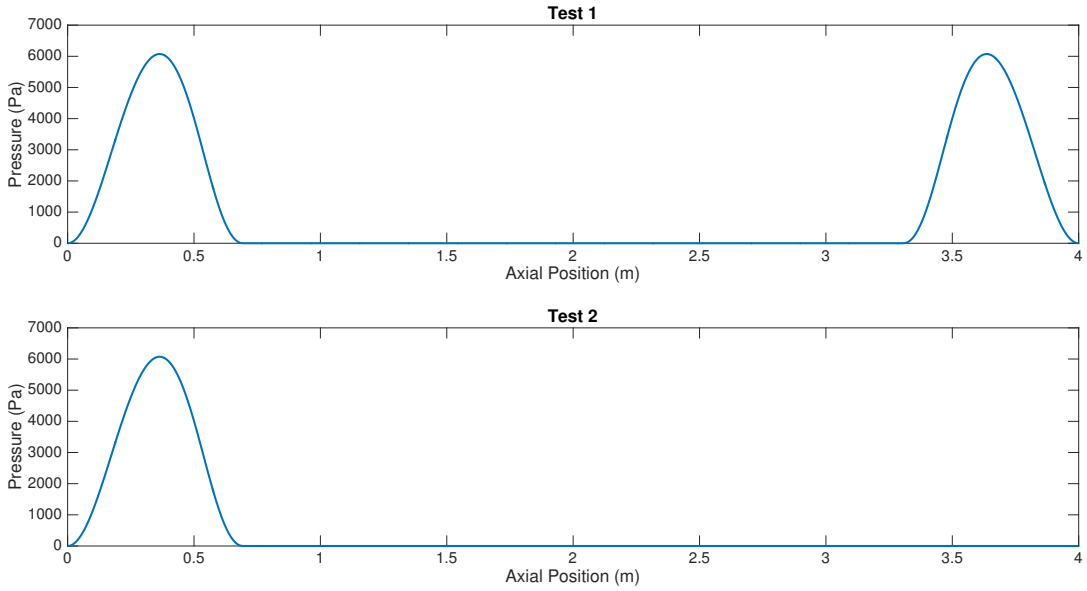

Figure 1: Top: Test 1 - the tube is excited from both ends. Bottom: Test 2 - the tube is excited only at the left hand side.

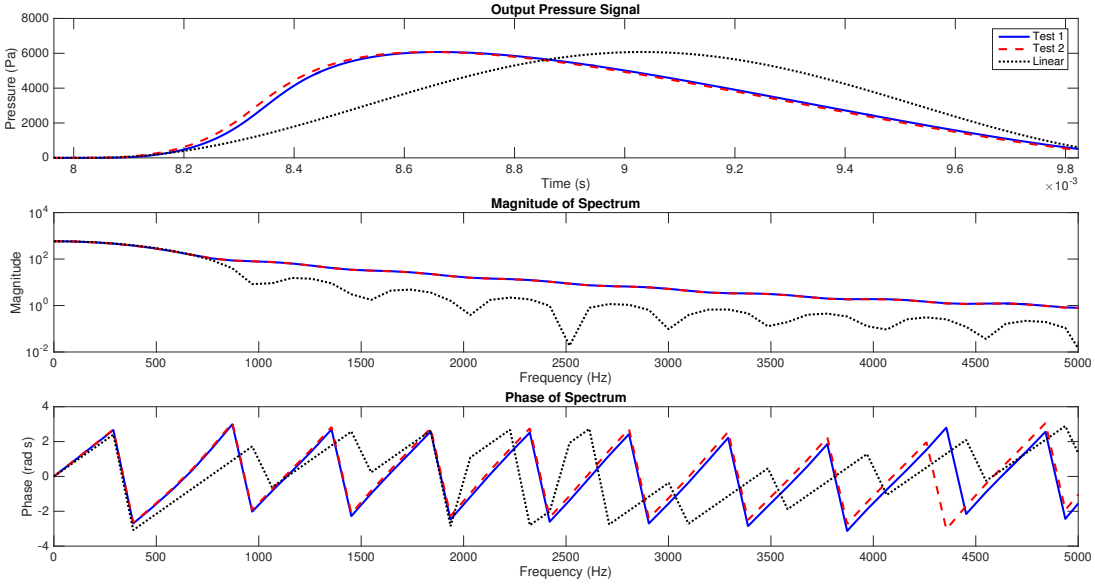

Figure 2: Top: Recorded time-pressure signal taken at $x = 2.8$ m for Test 1 (solid blue), Test 2 (dashed red), and using the linear system (dashed black). The graph has been enlarged around the pulse to make the separation between Test 1 and Test 2 visible. Middle: Magnitude of the the Fourier transform of the recorded pressure. Bottom: Phase of the Fourier transform.

at middle (magnitude) and bottom (phase) of Figure 2 (note that for Test 1, the initial recorded

impulse is zeroed so that only the right travelling pulse is analysed). Comparisons to simulations performed at higher sample rates (not presented here) show that the results presented are valid up to 5 kHz.

Both Test 1 and Test 2 show a deformation of pulse shape relative to the linear system and the magnitude of the spectrum is similar for both cases. This highlights the dominant cumulative effect of the nonlinearity that is larger than the local interaction between two waves [4]. In Test 1, the main body of the pulse arrives slightly behind that of Test 2. This is also shown in the phase plot at the bottom of Figure 2. The phase of Test 1 and Test 2 are similar up to around 2.5kHz. Above this, the phase of Test 2 relative to Test 1 starts to increase.

4 Case b: Scattering of waves at a change in cross section

In this section, the response of the models 1-3 to a change in cross sectional area is investigated. This is done by linearising the model equations, which are presented in Table 1, and performing dispersion analysis for a suitable bore profile.

Model 1 - Linearised Euler Equations (3)
$\partial_t p + \rho_0 c_0^2 \partial_x v + \rho_0 c_0^2 v \frac{S'}{S} = 0, \quad \partial_t v + \frac{1}{\rho_0} \partial_x p = 0$
Model 2 - Linearised Perturbation Model (9)
$\partial_t p + \rho_0 c_0^2 \partial_x v + \frac{c_0 p}{2} \frac{S'}{S} = 0, \quad \partial_t v + \frac{1}{\rho_0} \partial_x p + \frac{c_0 v}{2} \frac{S'}{S} = 0$
Model 3 - Linearised Velocity Wave Model (13)
$\partial_t p + \rho_0 c_0^2 \partial_x v + \rho_0 c_0^2 v \frac{S'}{S} = 0, \quad \partial_t v + \frac{1}{\rho_0} \partial_x p + \frac{p}{\rho_0} \frac{S'}{S} = 0$

Table 1: Linearised models presented in Section 2

4.1 Dispersion analysis

Consider the case of an exponential horn so that $S = S_0 e^{\alpha x}$ and $S'/S = \alpha$, where α is the flaring constant and S_0 is the the surface area at the opening of the tube. For all of the models under investigation, this particular bore profile allows solutions of the form $p = e^{j(kx+\omega t)}$, where k is the spatial wave number, ω is the angular frequency and $j = \sqrt{-1}$. The wave numbers for Model 1 are

$$k_{1\pm} = \frac{j\alpha \pm \sqrt{4\left(\frac{\omega}{c_0}\right)^2 - \alpha^2}}{2} \tag{17}$$

Similarly for Model 2 the wave number is

$$k_{2\pm} = \frac{\pm\sqrt{4\left(\frac{\omega}{c_0}\right)^2 - \alpha^2 - \frac{4j\alpha\omega}{c_0}}}{2} = \mp\frac{j\alpha}{2} \pm \frac{\omega}{c_0} \tag{18}$$

and for Model 3 the wave number is

$$k_{3\pm} = \frac{2j\alpha \pm \sqrt{4\left(\frac{\omega}{c_0}\right)^2}}{2} = j\alpha \pm \frac{\omega}{c_0} \tag{19}$$

For $\alpha = 0$, all models have the same wave number and have separable wave solutions — this corresponds to a cylindrical tube. For $\alpha > 0$, Model 1 no longer permits separable wave solutions and has a cut-off frequency, below which waves are spatially damped, and the real part of the wave number, when it exists, is modified by α (this is a standard result in acoustics). Models 2 and 3 always have a real part to their wave numbers which is not modified by α. This means that no cut-off behaviour exists in these models — waves are free to propagate in the tube and the amplitude of these waves are scaled by the cross sectional area. This is highlighted by rewriting Model 3 in second order form as $\partial_{tt}(Sv) - c_0^2\partial_{xx}(Sv) = 0$ which is the wave equation for the conserved quantity Sv; as S increases, v must decrease. When used to model an exponential horn, models 2 and 3 give resonances that are the same frequencies as those of a cylinder.

5 Conclusions

This paper is intended to highlight the effect of using separable wave solutions in nonlinear propagation models applied to musical acoustics. Starting with the linear case b), it has been shown that neglecting coupling between forwards and backwards waves can have a dramatic effect on the behaviour of the system. In practice, this can be rectified through the use of scattering junctions, as in the case of Digital Waveguides, or other similar methods. However, in the nonlinear case a), there is still a coupling between forwards and backwards waves through their wave speed.

The numerical experiments presented here show that a slight delay occurs when a low frequency wave passes a similar wave travelling in the opposite direction. It is not clear whether this would cause an audible difference to the produced sound, but it could change the frequencies of possible standing wave configurations that are produced within the instrument. This test has been performed for the equivalent of a perfectly reflected pulse of finite width, whereas under playing conditions the reflected wave would have a smaller magnitude due to radiation of sound from the instrument. However, the interaction would occur for a longer period of time once the standing waves have been established. Further tests are therefore required to test how important this interaction is and what effect the dynamic level, frequency, and duration of interaction has on the waves within the system.

Although results were acquired over a reasonable frequency range with scheme (16), the tests performed here are at the limit of the scheme's use — larger pressure signals or higher fre-

quency pulses begin to display numerical instabilities that result in exponential growth. Therefore further investigation is required into finding a stable scheme for this problem (if such a scheme exists). Losses associated with viscous and thermal effects have been neglected in this study but could be included into the model. This would reduce the amplitude of the signals and therefore reduce the effect of the nonlinearity and the severity of the numerical instabilities. Efficient, passive models for this process already exist [14] and could easily be included in the model.

Acknowledgements

This work was supported by the European Research Council under grant number ERC-2011-StG-2011-279068-NESS. Thanks go to Joël Gilbert, Bruno Lombard, Sylvain Maugeais and Christophe Vergez for their discussions on the models presented in this paper.

References

[1] S. Earnshaw, "On the mathematical theory of sound," *Philosophical Transactions of the Royal Society of London*, vol. 150, pp. 133–148, 1860.

[2] J. W. Beauchamp, "Analysis of simultaneous mouthpiece and output waveforms of wind instruments," in *The 66^{th} Audio Engineering Society Convention*, (Los Angeles), 1980.

[3] A. Hirschberg, J. Gilbert, R. Msallam, and A. P. J. Wijnands, "Shock waves in trombones," *Journal of the Acoustical Society of America*, vol. 99, no. 3, pp. 1754–1758, 1996.

[4] L. Menguy and J. Gilbert, "Weakly nonlinear gas oscillations in air-filled tubes; solutions and experiments," *Acustica - Acta Acustica*, vol. 86, pp. 798–810, 2000.

[5] L. Menguy, *Propagation Acoustique Non Lineaire Dans Les Guides Monodimensionnels*. PhD thesis, Universite du Maine, 2001.

[6] J. Gilbert, L. Menguy, and M. Campbell, "A simulation tool for brassiness studies(l)," *Journal of the Acoustical Society of America*, vol. 123, no. 4, pp. 1854–1857, 2008.

[7] B. Lombard, C. Vergez, and E. Cottenceau, "Modélibation de la propagation non linéaire avec pertes viscothermiques: application à la famill des cuivres," in *Proceedings of the Congres Francais d'Acoustique (CFA)*, (Poitiers, France), April 2014.

[8] M. W. Thompson and W. J. Strong, "Inclusion of wave steepening in a frequency-domain model of trombone sound production," *Journal of the Acoustical Society of America*, vol. 110, no. 1, pp. 556–562, 2001.

[9] C. Vergez and X. Rodet, "Trumpet and trumpet player: Model and simulation in a musical context," in *Proceedings of the International Computer Music Conference*, (La Habana, Cuba), 2001.

[10] W. Kausel and C. B. Geyer, "Time domain simulation of standing waves in brass wind instruments taking non-linear wave steepening into account," in *Proceedings of the Stockholm Music Acoustics Conference 2013*, (Stockholm, Sweden), 2013.

[11] J. O. Smith III, *Physical Audio Signal Procesing*. 2004. Draft version. Available online at `http://ccrma.stanford.edu/~jos/pasp04/`.

[12] P. G. LeFloch and M. Westdickenberg, "Finite energy solutions to the isentropic euler equations with geometric effects," *Journal de Mathématiques Pures et Appliquées*, vol. 88, no. 2, pp. 389–429, 2007.

[13] S. Bilbao and J. Chick, "Finite difference time domain simulation for the brass instrument bore," *Journal of the Acoustical Society of America*, vol. 134, no. 5, pp. 3860–3871, 2013.

[14] S. Bilbao, R. Harrison, J. Kergomard, B. Lombard, and C. Vergez, "Passive models of viscothermal wave propagation in acoustic tubes," *The Journal of the Acoustical Society of America*, vol. 138, no. 2, 2015.